

Zhengmiao Yuan^{1,2,3}, Wenqing Yang^{1,2,3,*}, Jianlin Xuan^{1,2,3}

¹ School of Aeronautics, Northwestern Polytechnical University, Xi'an 710072, China
² Research & Development Institute of Northwestern Polytechnical University in Shenzhen, Shenzhen 518057, China

³ National Key Laboratory of Aircraft Configuration Design, Xi' an 710072, China

Abstract

In recent years, flapping-wing micro-air vehicles (FMAVs) have garnered extensive attention from scholars due to their exceptional aerodynamic performance. However, conventional FMAVs cannot traverse certain terrains, significantly limiting their application in rescue, detection, and reconnaissance missions. This paper investigates a flying-crawling integrated FMAV. The FMAV is a nonlinear and non-stationary system characterized by nonlinear, time-varying, and highly coupled dynamics, posing significant challenges to its attitude control. This paper develops a serial PID attitude controller based on wind tunnel experiments, demonstrating superior tracking and control performance. The specific implementation is as follows: first, an aerodynamic model of the FMAV is established based on wind tunnel experiments. Secondly, a dynamics model is derived using single rigid body theory and small perturbation linearization. Finally, a serial PID attitude controller is designed based on the linearized dynamics model, and simulations are conducted to verify the controller's superior control performance. A novel methodology for the design of attitude controllers for flapping-wing vehicles is presented. The findings of this paper will facilitate the implementation of flying-crawling integrated FMAVs.

Keywords: Flapping wing, Flying-crawling integrated FMAV, Wind tunnel, Dynamic model, Attitude Control.

1. Introduction

The flight of birds in nature has inspired many researchers to design various flapping-wing micro-air vehicles (FMAVs) [1-3]. However, among the numerous FMAVs, only a few possess ground crawling capabilities, significantly limiting their potential applications. This paper introduces an FMAV with ground crawling capability, termed the flying-crawling integrated FMAV. To enhance the stability of the flying-crawling integrated FMAV, this paper explores its dynamic modeling and attitude control.

To date, many scholars have conducted research on FMAV control. However, due to their nonlinear and highly coupled characteristics, most current modeling methods for FMAVs are based on empirical models under the assumption of quasi-steady state theory [4]. Building on these empirical models, dynamic models and control strategies are studied [5-7]. Reference [8] proposed a dynamic linearization method based on a model-free adaptive control scheme. This method incorporates an anti-saturation compensator to prevent input saturation, enhancing the effectiveness of the model-free adaptive control scheme compared to conventional methods. Reference [9] established an accurate tail control model and designed the first corresponding controller through a comprehensive study of flight biomechanics, achieving effective pitch stabilization with good control performance by utilizing the flow caused by flapping. Reference [10] applied an agent model approach to establish the flapping and tail models of FMAV, and used these models in self-impedance control for FMAV attitude control, resulting in stable flight outcomes in flight experiments.

Compared with other works, this paper does not rely on a mathematical model under an empirical formulation. Instead, a more reliable dynamic model of the FMAV has been established through wind tunnel experiments. Based on this model, the attitude controller is designed, and the detailed sections are organized as follows.

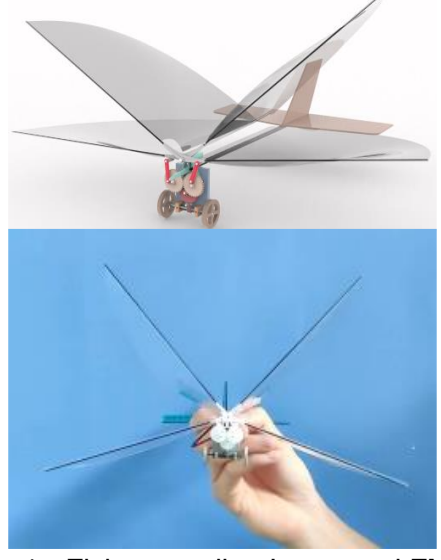
Section 2 describes the wind tunnel test procedure, the aerodynamic and dynamic modeling, and the attitude controller design, respectively. Section 3 explains the wind tunnel test results and the attitude

control simulation results. Section 4 summarizes the whole work.

2. Materials and Methods

2.1 The flying-crawling integrated FMAV

The flying-crawling integrated flapping-wing micro-air vehicle (FMAV), as depicted in Figure 1, consists of a propulsion device, flapping wings, wheels, fuselage, tail wings, and electronic components, as outlined in Table 1. Both lift and thrust required for flight are generated by the "X" flapping wings, while the propulsion for crawling is provided by the wheels. The propulsion device, illustrated in Figure 2, comprises a dual-crank dual-rocker mechanism and a worm gear-worm mechanism. The former achieves reciprocating flapping of the wings, while the latter imparts motion to the wheels. To maintain minimal weight, this design employs a single motor to drive both flying and crawling modes simultaneously.



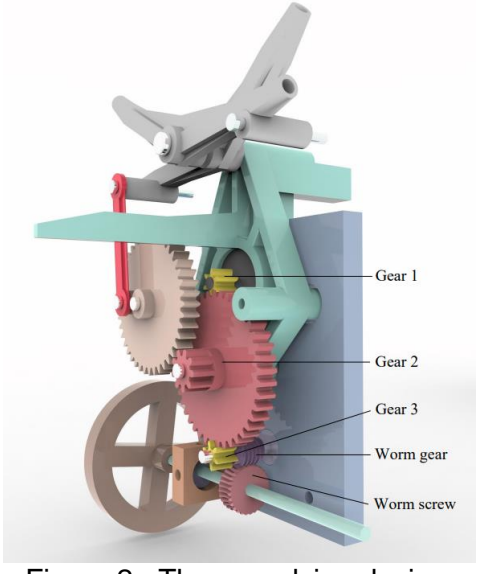


Figure 1 - Flying-crawling Integrated FMAV.

Figure 2 - The propulsion device.

Attitude control moments are achieved through the deflection of the tail wing control surfaces. The tail wing consists of a vertical stabilizer and elevator, as well as a horizontal stabilizer and rudder. Pitch moments are generated by controlling the elevator, while yaw moments are acquired through the manipulation of the rudder. During ground crawling, directional control is achieved by deflecting the rudder surfaces.

Table 1 - Basic information for Flying-crawling Integrated FMAV

Parameter	Value
Total mass of the FMAV	24.6g
Wing span	300mm
Flapping frequency	16HZ

2.2 Aerodynamic modeling

The objective of this section is to construct an aerodynamic model for the flying-crawling integrated FMAV, which will serve as the foundation for the subsequent dynamic model. The nonlinear nature of the aerodynamic forces and moments generated by FMAVs means that empirical formulas based on the quasi-steady-state model cannot be universally applied to all FMAVs. An experimental approach, therefore, offers greater accuracy and reliability. Accordingly, as illustrated in Figure 3, this paper presents a flow chart that employs wind tunnel experiments to construct the aerodynamic mode.

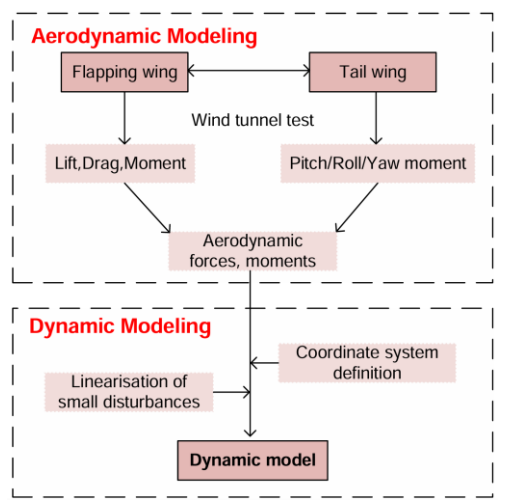


Figure 3 -The Process of dynamics modeling

2.3 Wind tunnel experimental design

The wind tunnel experimental system utilized in this paper is depicted in Figure 4. The system comprises an open-ended wind tunnel, a wind tunnel measurement and control system, an experimental measurement balance, and a data acquisition system. It is a low-speed open-ended jet wind tunnel, with an experimental section consisting of a circular section with a diameter of 1.8 meters. The turbulence within the experimental section is less than 0.5%, and the wind speed ranges from 4 to 15 m/s. The measurement and control system of the wind tunnel includes a wind speed control system and an angle control system, both of which are computerized, enabling the experimental state to be adjusted with great accuracy and speed.

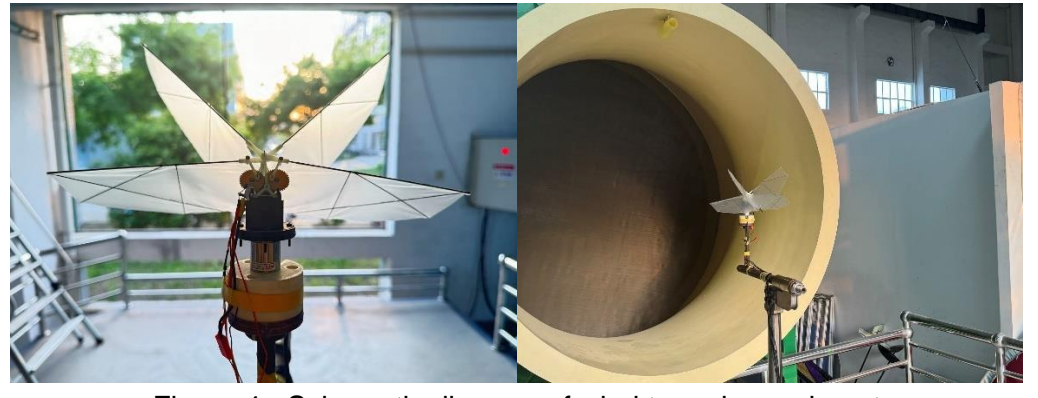


Figure 4 - Schematic diagram of wind tunnel experiment

To obtain a quantitative relationship that fully reflects the real aerodynamic forces and the experimental factors, it is necessary to adopt a full factorial experimental method. This method requires traversing all the states of all experimental factors, which increases the workload of the experiment to some extent. However, it can improve the accuracy of the established aerodynamic model. To construct a relatively accurate aerodynamic model using a limited number of experimental state points, it is necessary to select the experimental level of each experimental factor as closely as possible to the range of actual flight use under the conditions permitted by the experimental device. Consequently, the experimental factors and states selected for this experiment are presented in Table 2.

Table 2 - The variable setup employed in wind tunnel experiments.

Experimental factors	Value
Flow speed	4m/s、5m/s
Attack angle	0°、4°、8°、12°、16°、20°
Flapping frequency	8Hz、10Hz、12Hz、14Hz、16Hz、18Hz

Given that the research object of this paper belongs to the FMAV, the forces and moments generated by it are relatively small. Therefore, for the experimental force measurement balance, the six-axis force/moment sensor of the nano17 series from ATI Industrial Automation Co., Ltd. is selected, which

has a suitable range and high resolution. The device is suitable for the measurement of dynamic flutter aerodynamic forces generated by flapping wings.

2.3.1 Data processing and aerodynamic modeling

As the flapping wing undergoes a periodic reciprocating motion, the resulting aerodynamic force and moment exhibit strong nonlinear cyclic variation characteristics. This results in the up-and-down periodic sinking and floating motions of the FMAV during actual flight. This paper considers the aerodynamic model of the FMAV based on the cycle-averaged flight characteristics of the FMAV. However, it is important to note that the model does not take into account the sinking and floating motions caused by the flapping wing during a flapping cycle. Consequently, it is necessary to cycle-average the results measured in the wind tunnel experiments. A polynomial fit is then performed on the cycle-averaged results to obtain the aerodynamic model shown in Equation(1).

$$\begin{cases} L = -0.4527 + 0.3122f + 0.2081\alpha + 0.0753\alpha f - 0.0384\delta_e \\ M = -0.1858 + 0.0501V - 0.0112f + 0.0255\alpha - 0.0077V\alpha \\ -0.0019f\alpha - 0.0347\delta_e - 0.0517q \\ T = -18.108 + 4.1674V + 2.9287f + 0.11329\alpha - 0.80896Vf \\ -0.021835f\alpha - 0.044508f^2 + 0.022208Vf^2 + 0.0002\delta_e \end{cases}$$

$$(1)$$

where L is the cycle-averaged lift, M is the cycle-averaged pitching moment and T is the cycle-averaged thrust.

2.4 Dynamic modeling

Building upon the aerodynamic model established above, the dynamics model is further developed on this foundation. Given the complexity and nonlinearity of the FMAV, a series of assumptions are first made to facilitate the subsequent modeling work in this part.

- (1) The cycle-averaged assumption is introduced to consider only the average state change over a period of time during the flapping wing flight, thereby ignoring the fuselage sinking and vibration motions induced by the flapping.
- (2) It is assumed that the mass and mass distribution of the flapping-wing vehicle remain constant and exhibit a longitudinal plane of symmetry.
- (3) In the absence of consideration for the effects of the Earth's rotation and revolution, the curvature of the Earth is not accounted for, and the ground is treated as a flat surface.

2.4.1 Coordinate System

In order to describe the dynamics model of the FMAV three coordinate systems are established in this paper: the inertial coordinate system $Ox_g y_g z_g$, the body coordinate system $Ox_b y_b z_b$ and the aerodynamic coordinate system $Ox_w y_w z_w$.

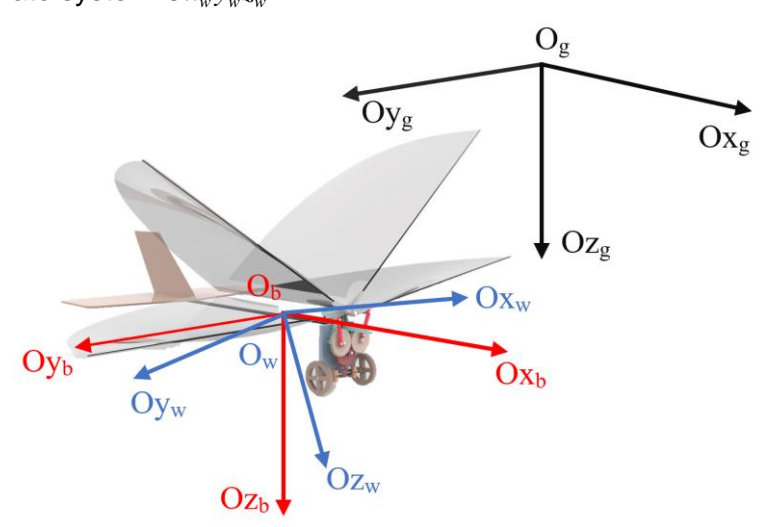


Figure 5 - Demonstration of all the coordinate systems

The inertial coordinate system $Ox_{e}y_{e}z_{e}$ is fixed to the Earth and utilizes the Northeast-Southeast-

Down (NED) coordinate system. The position and attitude of the vehicle, as well as its speed and acceleration, are expressed relative to this coordinate system.

The origin of the body coordinate system $Ox_b y_b z_b$ is situated at the center of mass of the FMAV. The Ox_b axis is situated in the plane of symmetry of the FMAV, parallel to the body axis and oriented in the direction of forward motion. The Oz_b axis is also in the plane of symmetry of the FMAV, perpendicular to the axis of the body and pointing to the bottom of the body. Finally, the Oy_b axis is perpendicular to the symmetry of the body and points to the right of the body. The body coordinate system is employed to describe the moment of inertia and product of inertia of the FMAV, as well as the roll, pitch and yaw moments to which the vehicle is subjected.

The origin of the aerodynamic coordinate system $Ox_w y_w z_w$ is located in the center of mass of the FMAV, with the Ox_w axis pointing to the direction of airspeed of the aircraft. The Oz_w axis is located in the symmetry plane of the FMAV, perpendicular to the Ox_w axis and pointing to the bottom of the body. Finally, the Oz_w axis is perpendicular to the $Ox_w z_w$ plane, pointing to the right side. The aforementioned coordinate system is employed primarily for the description of aerodynamic drag, lift and lateral force on FMAV. Furthermore, the aerodynamic model of FMAV is established within this coordinate system.

2.4.2 Dynamic modeling

motion for the FMAV.

The preceding assumptions pertain solely to the average flight characteristics of the FMAV over a specified period. Consequently, the dynamics of the FMAV can be modeled in terms of both translational and rotational motions with reference to the single rigid body dynamics model.

From the theoretical mechanics, the equations for the center-of-mass advection dynamics of the FMAV in the body-axis system can be established as follows:

$$\begin{cases} m(\frac{du}{dt} + qw - rv) = F_x \\ m(\frac{dv}{dt} + ru - pw) = F_y \\ m(\frac{dw}{dt} + pv - qu) = F_z \end{cases}$$
 (2)

Where u,v,w represent the three-axis components of the FMAV's inertial velocity vector in the body coordinate system. p,q,r represent the triaxial component of the FMAV's inertial angular velocity vector in the body coordinate system. F_x,F_y,F_z represent the three-axis component of the combined external force on the FMAV in the body coordinate system.

Given that the FMAV possesses a longitudinal plane of symmetry, the dynamical equations for the rotation around the center of mass of the FMAV in the body-axis system are as follows:

$$\begin{cases} M_{x} = I_{x} \frac{dp}{dt} + (I_{z} - I_{y})qr + I_{zx}(pq + \frac{dr}{dt}) \\ M_{y} = I_{y} \frac{dq}{dt} + (I_{x} - I_{z})rp + I_{zx}(r^{2} - p^{2}) \\ M_{z} = I_{z} \frac{dr}{dt} + (I_{y} - I_{x})pq + I_{zx} \left(\frac{dp}{dt} - qr\right) \end{cases}$$
(3)

Where M_x, M_y, F_z represent the three-axis component of the combined external moment applied to the FMAV in the body coordinate system. I_x, I_y, I_z represent the triaxial moment of inertia of the FMAV. I_{zx} represent the product of inertia of the FMAV with respect to the longitudinal plane of symmetry. The coordinate transformations permit the derivation of the translational and rotational equations of

$$\begin{bmatrix} \dot{x}_g \\ \dot{y}_g \\ \dot{z}_g \end{bmatrix} = \begin{bmatrix} \cos\theta\cos\psi & (\sin\phi\sin\theta\cos\psi - \cos\phi\sin\psi) & (\cos\phi\sin\theta\cos\psi + \sin\phi\sin\psi) \\ \cos\theta\sin\psi & (\sin\phi\sin\theta\sin\psi + \cos\phi\cos\psi) & (\cos\phi\sin\theta\sin\psi - \sin\phi\cos\psi) \\ -\sin\theta & \sin\phi\cos\theta & \cos\phi\cos\theta \end{bmatrix} \begin{bmatrix} u \\ v \\ w \end{bmatrix}$$
 (4)

Where x_e, y_e, z_e represents the coordinates of the FMAV's spatial position.

$$\begin{bmatrix} \dot{\phi} \\ \dot{\theta} \\ \dot{\psi} \end{bmatrix} = \begin{bmatrix} p + (q\sin\phi + r\cos\phi)\tan\theta \\ q\cos\phi - r\sin\phi \\ (q\sin\phi + r\cos\phi)/\cos\theta \end{bmatrix}$$
 (5)

Where ϕ, θ, ψ represents the FMAV attitude Euler angle

2.4.3 Linearization of equations and state spaces

The system of kinetic equations solved above is a nonlinear system of equations for which an analytical solution cannot be obtained in general. Therefore, it is necessary to linearize the system of nonlinear dynamic equations under the small perturbation assumption. The linearized system of equations can be divided into transverse and longitudinal equations of motion.

As the aerodynamic model is constructed within the aerodynamic coordinate system and the dynamic model within the body coordinate system, it is essential to define the relationship between the velocity vector [V,0,0] within the aerodynamic coordinate system and the velocity vector [u,v,w] within the body coordinate system.

$$\begin{bmatrix} u \\ v \\ w \end{bmatrix} = \begin{bmatrix} \cos \alpha \cos \beta & -\cos \alpha \sin \beta & -\sin \alpha \\ \sin \beta & \cos \beta & 0 \\ \sin \alpha \cos \beta & \sin \alpha \sin \beta & \cos \alpha \end{bmatrix} \cdot \begin{bmatrix} V \\ 0 \\ 0 \end{bmatrix}$$
 (6)

The levelling point measured by the wind tunnel experiment is selected as the base state of a small perturbation, and then a state quantity can be obtained by superimposing the small perturbation state on the base state.

$$V = V_0 + \Delta V \quad \alpha = \alpha_0 + \Delta \alpha \quad \beta = \Delta \beta$$

$$p = \Delta p \quad q = \Delta q \quad r = \Delta r$$

$$u = u_0 + \Delta u \quad v = v_0 + \Delta v \quad w = w_0 + \Delta w$$

$$\phi = \Delta \phi \quad \theta = \theta_0 + \Delta \theta \quad \psi = \Delta \psi$$

$$(7)$$

Where $p_0 = q_0 = r_0 = \beta_0 = \phi_0 = \psi_0 = 0$. X_0 represent the base motion quantity of each state quantity. Δ_i represent the amount of perturbation of each state quantity.

It can be demonstrated that, under the assumption of a small perturbation, the derivatives of the longitudinal aerodynamic forces and moments with respect to the transverse lateral parameters are all equal to zero at their base state of motion. A similar conclusion can be drawn for the derivatives of the transverse lateral aerodynamic forces and moments with respect to the longitudinal parameters, which are also equal to zero in their reference motion state.

Therefore, based on the above assumptions and the aerodynamic model developed in this paper, the longitudinal aerodynamic model of the linearized FMAV can be derived as shown in Equation (8).

$$\begin{cases} \Delta L = L_{V} \Delta V + L_{\alpha} \Delta \alpha + L_{f} \Delta f + L_{\delta_{e}} \Delta \delta_{e} \\ \Delta T = T_{V} \Delta V + T_{\alpha} \Delta \alpha + T_{f} \Delta f + T_{\delta_{e}} \Delta \delta_{e} \\ \Delta M_{y} = M_{y,V} \Delta V + M_{y,\alpha} \Delta \alpha + M_{y,f} \Delta f + M_{y,\delta_{e}} \Delta \delta_{e} + M_{y,q} \Delta q \end{cases}$$
(8)

Where X_i represents the derivative of the aerodynamic force or moment with respect to the reference state or control quantity.

The joint equation (1-6), which retains its longitudinal equation solution, can be expressed as follows:

$$\begin{cases} \Delta \dot{V} = \frac{1}{m} \Delta T + g(\Delta \alpha - \Delta \theta) \\ \Delta \dot{\alpha} = \Delta q - \frac{\Delta L}{mV_0} \\ \Delta \dot{q} = \frac{\Delta M_y}{I_y} \\ \Delta \dot{\theta} = \Delta q \end{cases}$$
(9)

The joint equation (7-8) can be expressed as follows.

$$\begin{bmatrix} \Delta \dot{V} \\ \Delta \dot{\alpha} \\ \Delta \dot{q} \\ \Delta \dot{\theta} \end{bmatrix} = \begin{bmatrix} \frac{T_{V}}{m} & \frac{T_{\alpha} + mg}{m} & 0 & -g \\ \frac{L_{V}}{mV_{0}} & \frac{L_{\alpha}}{mV_{0}} & 1 & 0 \\ \frac{M_{y,V}}{I_{y}} & \frac{M_{y,\alpha}}{I_{y}} & \frac{M_{y,q}}{I_{y}} & 0 \\ 0 & 0 & 1 & 0 \end{bmatrix} \begin{bmatrix} \Delta V \\ \Delta \alpha \\ \Delta q \\ \Delta \theta \end{bmatrix} + \begin{bmatrix} \frac{T_{f}}{m} & \frac{T_{\delta_{c}}}{m} \\ \frac{L_{f}}{mV_{0}} & \frac{L_{\delta_{c}}}{mV_{0}} \\ \frac{M_{y,f}}{I_{y}} & \frac{M_{y,\delta_{e}}}{I_{y}} \end{bmatrix} \begin{bmatrix} \Delta f \\ \Delta \delta_{e} \end{bmatrix}$$

$$(10)$$

Substitution of the results of the linearization result into Equation (10) yields. As shown in Equation(11), we obtain the small perturbation equations of motion for the FMAV in the baseline constant straight level flight state of motion v = 4m/s, f = 16HZ, $\alpha = 16^{\circ}$. We will then use this small perturbation equation of motion as the object for the design of the attitude controller.

$$\begin{bmatrix} \Delta \dot{V} \\ \Delta \dot{\alpha} \\ \Delta \dot{q} \\ \Delta \dot{\theta} \end{bmatrix} = \begin{bmatrix} -103.0233 & 17.6667 & 0 & -9.8 \\ 0 & 11.7742 & 1 & 0 \\ 324.8889 & -158.6667 & -229.7778 & 0 \\ 0 & 0 & 1 & 0 & \Delta \theta \end{bmatrix} \begin{bmatrix} \Delta V \\ \Delta \alpha \\ \Delta q \\ \Delta \theta \end{bmatrix} + \begin{bmatrix} 25.41 & 0.0067 \\ 12.6417 & -0.32 \\ -166.4 & -138.8 \\ 0 & 0 \end{bmatrix} \begin{bmatrix} \Delta f \\ \Delta \delta_e \end{bmatrix}$$
 (11)

2.5 Attitude control design

Since the aerodynamic force of the FMAV is closely related to the flight attitude, it is necessary to complete the design of the attitude controller to ensure a stable vehicle attitude. The FMAV maneuver system designed in this paper includes longitudinal elevator and rudder maneuvers as well as lateral rudder maneuvers. This section will be based on the longitudinal FMAV dynamics model established above to complete the pitch channel attitude controller design. The controller architecture is depicted in Figure 6.

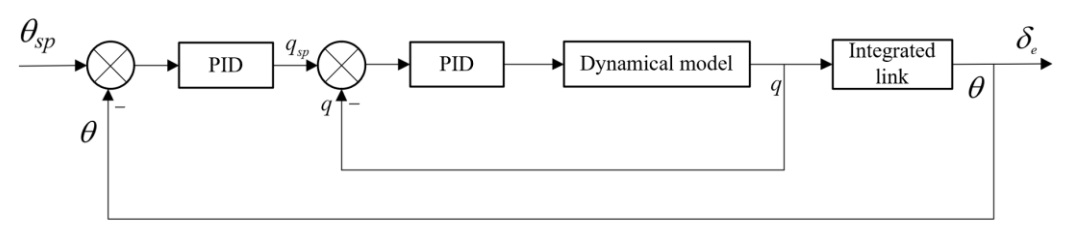


Figure 6 - The controller architecture.

A serial PID control algorithm is employed to design the attitude controller, which comprises an angle control loop and an angular velocity control loop. The actual attitude angle θ of the FMAV is fed back to the input $\theta_{\rm sp}$, and the difference between this and the desired attitude angle is then fed through the angle control loop PID controller to obtain the desired angular velocity value $q_{\rm sp}$. The difference between the desired angular velocity value and the feedback value q is then fed through the angular velocity loop PID controller to provide the dynamic model input δ_e . The algorithm is relatively simple in structure and exhibits good robustness. The transfer function $\Delta q/\Delta \delta_e$ from elevator maneuver to pitch angle velocity can be obtained from Equation (11) .the angular velocity control loop is regulated by means of the PI control rate, as illustrated in equation (12).

$$\delta_e = K_p^q \cdot (q_{sp} - q) + K_i^q \cdot \int (q_{sp} - q) dt \tag{12}$$

Where the gain coefficient K_p^q of the proportional control link of the pitch angle speed loop, the gain coefficient K_i^q of the integral control link of the pitch angle speed loop, and the pitch angle speed setpoint value q_{sp} and the pitch angle speed real-time value q, respectively, are the variables under consideration. Concurrently, the angle loop employs a PID controller with a control rate as indicated by equation 9.

$$q_{sp} = K_p^{\theta} \cdot (\theta_{sp} - \theta) + K_i^{\theta} \cdot \int (\theta_{sp} - \theta) dt + K_d^{\theta} \frac{d(\theta_{sp} - \theta)}{dt}$$
(13)

Where: K_p^{θ} is pitch angle loop proportional control link gain coefficient. K_i^{θ} is pitch angle loop integral control link gain coefficient. K_d^{θ} is pitch angle loop differential control link gain coefficient. θ_{sp} and θ represent the pitch loop proportional control link gain coefficients, which indicate the pitch angle set value and the real-time pitch angle value, respectively. The values of the PID parameters for the outer and inner loop, respectively, are presented in Equation (14).

$$K_p^q = 6, K_i^q = 6$$

 $K_p^\theta = 100, K_i^\theta = 1, K_d^\theta = 3$ (14)

3. Results and Discussion

3.1 Aerodynamic Results of Wind Tunnel Experiments

In this section, the cycle-averaged aerodynamic results of the flying-crawling integrated FMAV are presented. Due to the large amount of experimental data, the experimental results at the experimental state point v=4m/s, which is close to the actual flight reference state, are selected for analysis in this paper.

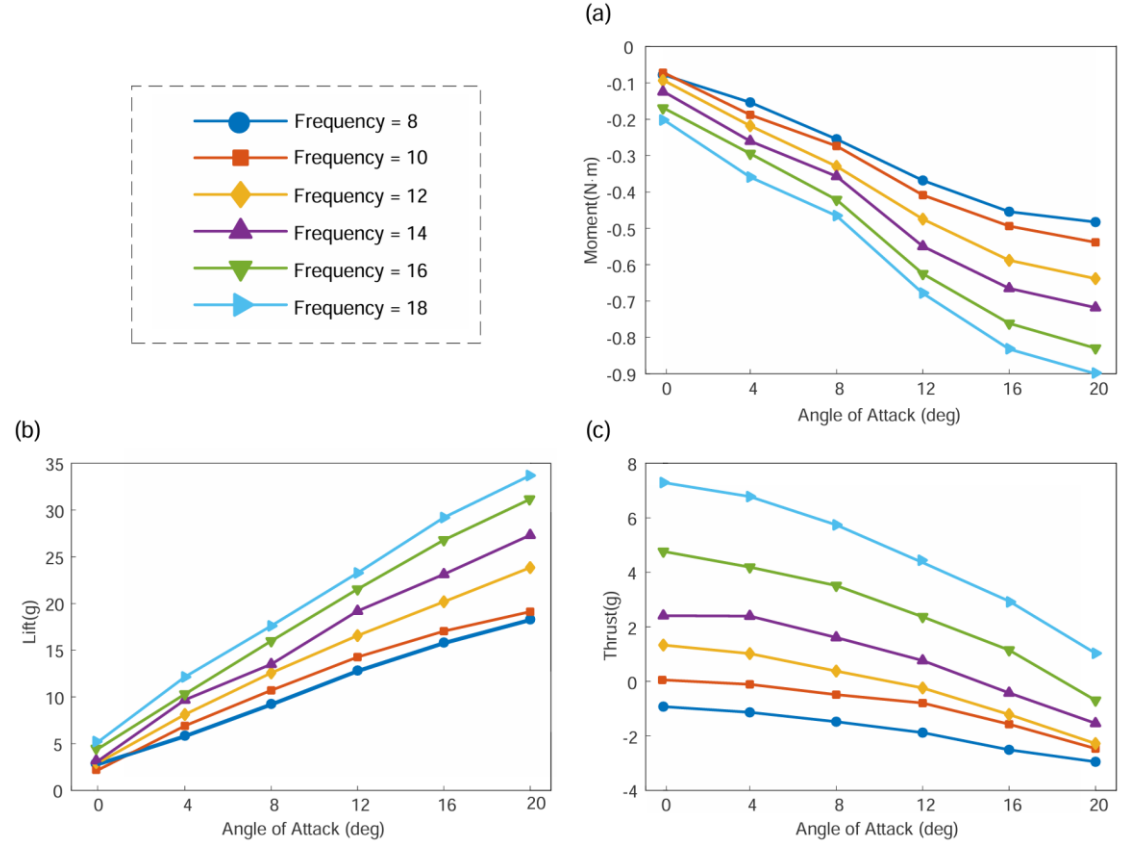


Figure 7 - Wind tunnel tests are used to investigate the effect of different conditions on the aerodynamic force generated by the flapping wing. (a)The effect of angle of attack and flapping frequency on pitching torque. (b)The effect of angle of attack and flapping frequency on lift. (c)The effect of angle of attack and flapping frequency on thrust.

The relationship between pitching moment and flapping frequency and angle of attack is shown in Figure 7(a). It can be seen that the average pitching moment is approximately linearly related to the

angle of attack, and the greater the angle of attack, the greater the average pitching moment, which is more evident at high flapping frequencies. The average pitching moment is also linearly related to the flapping frequency, and the higher the flapping frequency, the higher the pitching moment, which is more evident at high angles of attack.

Figure 7(b) shows the relationship between lift and flapping frequency and angle of attack. As the angle of attack and flapping frequency increase, the lift increases linearly. This is because as the angle of attack increases, the aerodynamic force generated by the X-wing from the 'clap-fling' mechanism is decomposed in the direction of the lift, and the greater the angle of attack, the greater the decomposed force. At the same time, as the angle of attack increases, the wing can be considered as a flat wing, which also generates increased lift under the action of the incoming flow, and the combined effect of the two is that the lift becomes greater as the angle of attack increases. The aerodynamic force generated by the 'clap-fling' mechanism also increases linearly with increasing flapping frequency. This also results in a linearly increasing relationship between lift and flapping frequency.

Figure 7(c) shows the average thrust versus flapping frequency and angle of attack. The average thrust is mainly generated by the horizontal component of the aerodynamic force generated by the 'clap-fling' mechanism. This also means that as the angle of attack increases, less force is converted into thrust. In total, when flying at v = 4m/s, $f \ge 16HZ$, $\alpha \ge 16^{\circ}$, it is capable of generating more than 25g of lift, along with about 2g of thrust, which is more than enough to meet the conditions for vehicle flight.

3.2 Attitude controller simulation results

In order to verify the control effect of the designed serial PID controller, an attitude control simulation based on the longitudinal small perturbation equation was constructed. A PID feedback control simulation was also constructed for comparison. The response curves of the two simulations under a given step signal are shown in Figure 8. From the figure, it can be seen that the response of the simulated system under the action of the PID controller has an overshoot of approximately 30%, stabilizing at 1.5 seconds with no steady state error. In contrast, the overshoot of the system under the action of the serial PID controller is only 5%, converging at 0.5 seconds with no steady state error. A comparison of the two responses reveals that the serial PID controller exhibits a smaller overshoot, faster response speed, and no steady state error. Furthermore, the serial PID controller demonstrates superior control efficacy and is capable of effectively regulating the pitch angle attitude.

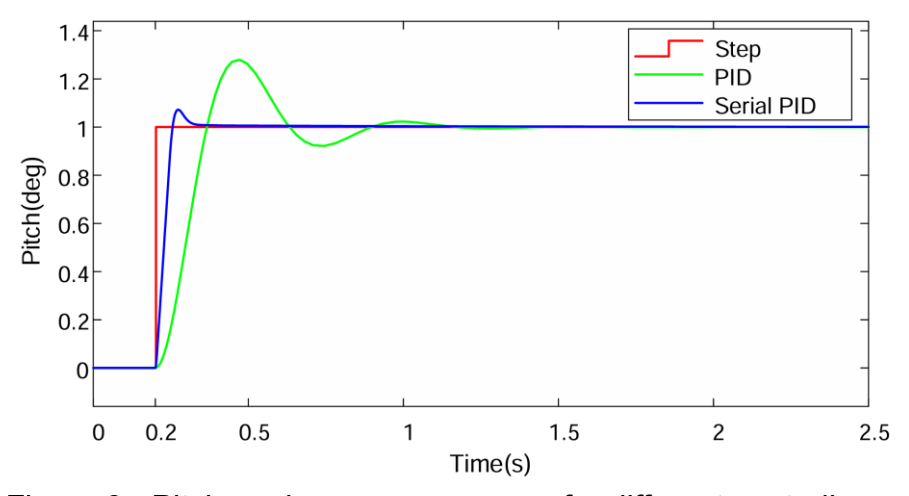


Figure 8 - Pitch angle response curves for different controller actions.

4. Conclusion

In order to enhance the flight stability of the flying-crawling integrated FMAV, we presents a comprehensive design for the attitude controller. The primary objective is to establish an aerodynamic model for the FMAV, which is achieved through wind tunnel testing. This model is then used to construct a dynamics model of the FMAV, which is based on the six-degree-of-freedom equations of motion and the small perturbation linearization method. Finally, a serial PID controller is designed for the attitude control of the FMAV. The simulation results demonstrate that the serial PID attitude controller, as designed in this paper, is capable of tracking input signals effectively and exhibiting high

control accuracy. In the future, we will conduct a flight test to ascertain the efficacy of this controller in a real-world setting.

5. Contact Author Email Address

Mailto: yangwenqing@nwpu.edu.cn

6. Copyright Statement

The authors confirm that they, and/or their company or organization, hold copyright on all of the original material included in this paper. The authors also confirm that they have obtained permission, from the copyright holder of any third party material included in this paper, to publish it as part of their paper. The authors confirm that they give permission, or have obtained permission from the copyright holder of this paper, for the publication and distribution of this paper as part of the ICAS proceedings or as individual off-prints from the proceedings

7. Acknowledgements

This study was supported by the National Natural Science Foundation of China (No. 52275293) and the Guangdong Basic and Applied Basic Research Foundation, China (No. 2023A1515010774).

8. References

- [1] Chin Y W, Kok J M, Zhu Y Q, et al. Efficient flapping wing drone arrests high-speed flight using post-stall soaring. Science Robotics, Vol. 5, No. 44, pp eaba2386, 2020.
- [2] Folkertsma G A, Straatman W, Nijenhuis N, et al. Robird: a robotic bird of prey. IEEE robotics & automation magazine, Vol. 24, No. 3, pp 22-29, 2017.
- [3] Pan E, Xu H, Yuan H, et al. HIT-Hawk and HIT-Phoenix: Two kinds of flapping-wing flying robotic birds with wingspans beyond 2 meters. Biomimetic Intelligence and Robotics Vol. 1, pp 100002, 2021.
- [4] Dickinson M H, Lehmann F O, Sane S P. Wing rotation and the aerodynamic basis of insect flight. Science, Vol. 284, No. 5422, pp 1964-1960, 1999.
- [5] Siqi W, Bifeng S, Ang C, et al. Modeling and flapping vibration suppression of a novel tailless flapping wing micro air vehicle. Chinese Journal of Aeronautics, Vol. 35, No. 3, pp 309-328, 2022.
- [6] He G, Su T, Jia T, et al. Dynamics analysis and control of a bird scale underactuated flapping-wing vehicle, IEEE Transactions on Control Systems Technology, Vol. 28, No. 4, pp 1233-1242, 2019.
- [7] He W, Yan Z, Sun C, et al. Adaptive Neural Network Control of a Flapping Wing Micro Aerial Vehicle with Disturbance Observer. IEEE Transactions on Cybernetics, Vol. 47, No. 10, pp 3452-3465, 2017.
- [8] Wang T, Jin S, Hou Z. Model free adaptive pitch control of a flapping wing micro aerial vehicle with input saturation//2020 IEEE 9th Data Driven Control and Learning Systems Conference (DDCLS). IEEE, 627-632, 2020.
- [9] Wang L, Jiang W, Wu Z, et al. Modeling the Bio-Inspired Wing-Tail Interaction Mechanism and Applying It in Flapping Wing Aircraft Pitch Control. IEEE Robotics and Automation Letters, Vol. 8, No. 5, pp2914-2921, 2023.
- [10]Liang S, Song B, Xuan J, et al. Active disturbance rejection attitude control for the dove flapping wing micro air vehicle in intermittent flapping and gliding flight. International Journal of Micro Air Vehicles, Vol.12, pp 1756829320943085, 2020.